J. Fluid Mech. (1999), *vol.* 385, *pp.* 1–20. Printed in the United Kingdom

© 1999 Cambridge University Press

Numerical simulation of converging nonlinear wavefronts

By PHOOLAN PRASAD AND K. SANGEETA†

Department of Mathematics, Indian Institute of Science, Bangalore 560 012, India
email: prasad@math.iisc.ernet.in

(Received 12 July 1996 and in revised form 31 July 1998)

The propagation of a two-dimensional weakly nonlinear wavefront into a polytropic gas in a uniform state and at rest has been studied. Successive positions of the wavefront and the distribution of amplitude on it are obtained by solving a system of conservation forms of the equations of weakly nonlinear ray theory (WNLRT) using a TVB scheme based on the Lax–Friedrichs flux. The predictions of the WNLRT are found to be qualitatively quite different from the predictions of the linear theory. The linear wavefronts leading to the formation of caustics are replaced by nonlinear wavefronts with kinks. By varying the initial shape of the wavefront and the amplitude distribution on it, the formation and separation of kinks on the wavefront has been studied.

1. Introduction

The propagation of a point on a pulse in one space dimension, say in the direction of the x-axis, represents a simple example of plane wavefront propagation. In this case a wavefront is a plane passing through any point on the pulse and parallel to the (y, z)-plane. Theory of propagation of such a wavefront, under the high-frequency approximation whether linear or nonlinear, is quite well known. In the case of latter when the system is governed by a hyperbolic system of homogeneous quasi-linear equations with coefficients given as functions of dependent variables, it is given by the theory of simple waves. Theory of propagation of a curved wavefront is quite complex. A simple example is a continuous set of wavefronts generated by a curved piston starting with zero initial velocity and going through small-amplitude motion in a polytropic gas. If nonlinearity of the governing equations is included, it may happen that the nonlinear waves from behind may overtake the ones in front of them leading to the formation of a curved shock.

In this paper, we study the successive positions of a single nonlinear wavefront (from a succession of wavefronts produced by the piston), which may interact with a shock and disappear from the flow field. However, there will always be a continuous set of wavefronts behind the shock and we strongly believe that the geometry of nonlinear wavefronts and the shock front will be qualitatively similar. In order that the high-frequency assumption is satisfied, a length scale associated with the piston motion should be small compared to the principal radii of curvature of the piston. In the high-frequency approximation, the leading terms give a solution in which the amplitude and phase are separated. The phase function satisfies a first-order

† Present address: CSIR-Centre for Mathematical Modelling and Computer Simulation, Bangalore 560 037, India.

https://doi.org/10.1017/S0022112098003310 Published online by Cambridge University Press

nonlinear partial differential equation which is called eikonal equation. The level surfaces of the phase function give the one-parameter family of curved wavefronts. In the high-frequency approximation, one considers the propagation of one of these wavefronts.

The characteristic curves of the eikonal equation are defined as rays, along which the transport equation is obtained for the amplitude. In the leading-order terms of linear theory, the ray equations decouple from the transport equation so that the rays starting from an initially concave wavefront envelope a caustic surface on which the amplitude tends to infinity, showing that the high-frequency assumption breaks down.

Experimental results (Sturtevant & Kulkarny 1976) and theoretical investigations (Whitham 1974; Prasad 1993) have shown that the amplitude of the wavefront has important effects on its geometry. There are two nonlinear ray theories, both based on small-amplitude assumption. The first one developed by Choquet-Bruhat (1969) (and also independently by Parker 1969, 1971) uses linear rays and nonlinearity is taken into account by stretching the linear rays in the longitudinal direction (i.e. along the linear rays) due to the dependence of ray velocity on the wave amplitude. Since the linear rays meet at the points of the caustic, this theory also breaks down much before the caustic is reached where again as in the linear theory the amplitude tends to infinity.

The second weakly nonlinear ray theory† developed by us (Prasad 1975, 1993, 1994), is valid over much larger length and time scales. We abbreviate this theory as WNLRT. In this theory the wave amplitude correction is incorporated in the eikonal equation itself and this leads to a system of ray equations coupled to the transport equation. The theory shows that the nonlinear rays stretch due to the dependence of the ray velocity on the wave amplitude, as in the work of Choquet-Bruhat, but in addition the wavefront rotates due to the non-uniform distribution of amplitude on the wavefront, so that the linear rays deviate from the nonlinear rays. In fact the two nonlinear effects, namely elongation of the rays (produced by the wave amplitude) and the deviation of the rays from linear rays (produced by the gradient of the wave amplitude along the wavefront) are jointly responsible for the resolution of the linear caustic (an example of a linear caustic is shown in figure 1, Friedlander 1958). If we take a converging nonlinear wavefront, the caustic plays no role in this solution. The main issue is not to find the solution near the caustic, because the caustic itself does not appear during the course of propagation of a curved nonlinear wavefront (see also the comment at the end of § 4), but to compute the wavefronts representing an entirely new phenomenon. This new phenomenon is the result of the coupling of the transport equation with the nonlinear ray equations; in this the wave amplitude remains small but finite and the caustic is replaced by a pair of kinks on the nonlinear

† We point out here that there are two types of nonlinear wavefronts. Nonlinear wavefronts arising in a compression pulse, which correspond to $M > 1$ (see (2.1) in the next section) and nonlinear wavefronts in an expansion wave which correspond to $M < 1$. In the first case the characteristics of the governing equations on the wavefront are real and in the second case they are complex (Ravindran & Prasad 1985; Prasad 1993). The results on the nature of the singularities on an expansion nonlinear wavefront are not yet clear. In this paper, we refer to nonlinear wavefronts only in a compression pulse, i.e. when $M > 1$. Note that the equations for the propagation of a shock front are different from those used in this paper for a single nonlinear wavefront. Though we mention some results on the shocks in earlier papers, it is only for refering to similar results or approach. Our aim here is to study a single nonlinear wavefront from a one-parameter family of fronts given by the level surfaces of the phase function. The results for a shock front will be qualitatively similar and hence the study of nonlinear wavefront is important.

https://doi.org/10.1017/S0022112098003310 Published online by Cambridge University Press

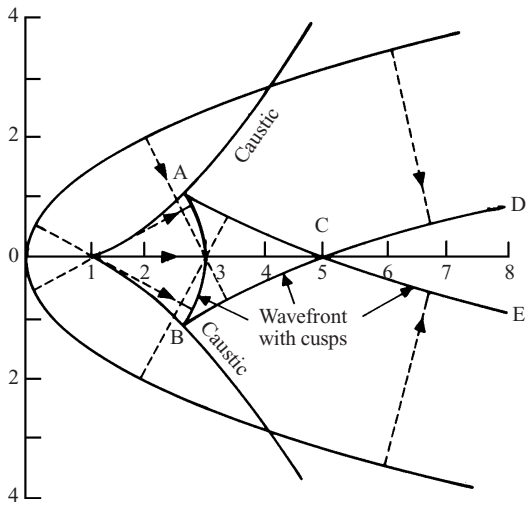


FIGURE 1. An initially smooth linear wavefront folds with a cusp type of singularity on a caustic. Rays are straight lines orthogonal to the wavefront.

wavefront (Prasad 1993, 1995). Across a kink, the wave amplitude and the direction of the normal to it are discontinuous.

The existence of a kink was first shown theoretically by Whitham in 1957 (see also Whitham 1974) in his theory of shock dynamics. He named a kink on a shock front a shock-shock. However, it is important to emphasize that Whitham did not study propagation of a nonlinear wavefront but that of a shock front. The first experimental results showing kinks on a shock front in a gaseous media were obtained by Sturtevant & Kulkarny (1976) and even today it is a great challenge to verify various observed properties of the flow field, containing these kinks, especially the transition from the shock fronts (or nonlinear wavefronts) containing kinks to linear acoustic fronts containing cusps. However, our aim here is not to study this transition from a nonlinear wavefront to a linear wavefront but to study numerically the solution of the equations of WNLRT containing the kinks. The WNLRT is not valid in the entire range of parameters required to study this transition.

The formation of singularities on the nonlinear wavefront was also observed by Ramanathan (1985), while solving the differential forms (i.e. forms which are not conservation laws) of the nonlinear ray equations. But the differential forms of the nonlinear ray equations can be used to study the propagation of the wavefront only till the singularities are formed because up to this time either the solution is smooth or has discontinuities in higher-order derivatives. But as soon as a singularity, i.e. a kink, appears on the wavefront, a discontinuity in the amplitude and in the normal direction comes into play. Kevlahan (1994, 1996) studied the propagation of a converging shock front in non-uniform flows in terms of a shock manifold equation together with compatibility conditions for shock strength and its normal derivative behind the shock, which in a suitable approximation form a closed set of differential equations similar to the differential forms of the nonlinear ray equations. Again the solutions could be obtained only till the kinks (shock-shocks) form on the shock front. For short times after the formation of kinks the solution was extended by propagating the shock disk and wings as separate shocks. The position of the kink at a later time was given by the intersection of the two shocks. But this intersection

https://doi.org/10.1017/S0022112098003310 Published online by Cambridge University Press

method gives a rough estimate of the shape and strength of the shock which may change considerably over time. Therefore, to study the propagation of kinks on a shock front for a large time one should use the conservation form of the shock ray equations as we do in this paper to study the propagation of a kink on a nonlinear wavefront. Two such sets of physically realistic conservation forms of the nonlinear ray equations were derived by Morton, Prasad & Ravindran in 1992 (see also Prasad 1993). Their derivation of conservation laws is included in the next section.

Even though we are dealing in this paper only with weakly nonlinear wavefronts, we would like to make one more comment on shock fronts. This is to answer the question: Can the WNLRT be shown formally to be an approximation to the propagation of weak shocks in some limit? For a nonlinear wavefront or a shock front propagating in a medium in a uniform state, there are two non-dimensional parameters. One is the ratio of the length scale in the normal direction over which significant change in the flow variables takes place to the principal radii of curvature of the front. When this parameter, let us call it ϵ, is small the high-frequency approximation is satisfied. The second is a non-dimensional measure of the amplitude of the wave, let us call it δ. The WNLRT is valid when these two parameters are of the same order. In this case, though a weakly nonlinear wavefront and a weak shock front have qualitatively the same geometrical features (we have extensive numerical results on the propagation of a weak shock which will be included in another paper), one cannot obtain the WNLRT as an approximation of a weak shock ray theory. However, there is a relation between them as given by Theorem 4.3, p. 74 of Prasad (1993) which briefly means that the propagation and physical properties of a weak shock front is the mean of those of a linear wavefront and a weakly nonlinear wavefront. This relation is valid only locally, i.e. in any small time interval. When the parameter ϵ is small and δ/ϵ is also small, both the WNLRT and shock ray theory are expected to give results close to the linear theory. Our WNLRT is not valid in this domain of parameters, which is important in order to study the transition from the WNLRT to linear theory.

In this paper we present results of extensive numerical solutions of the system of conservation laws of WNLRT for quite general initial data by which the initial shape of the wavefront and the initial value of the Mach number M prescribed on it can be varied to produce a large number of interesting cases. A total variation bounded scheme based on the Lax–Friedrichs flux has been used to solve the system of conservation laws. Thus the present work is a numerical investigation using the conservation forms of the WNLRT equations to study the detailed history of a wavefront which is either initially concave or has a periodic shape. Effects of varying initial curvature as well as the effect of varying initial Mach strength on the formation and separation of kinks have been studied. Some of the questions we address here are: (i) How does the separation of the kinks depend on the initial Mach strength? (ii) How does the time at which kinks are formed depend on M and initial curvature? (iii) How does the maximum Mach strength depend on the initial Mach strength? It is expected that this numerical investigation will give some understanding of a very complex phenomenon.

2. Governing equations

The geometry and position of a weakly nonlinear wavefront at a later time depends on its initial geometry and the initial distribution of intensity on it. Its motion is governed by a coupled system of ray equations and a transport equation (Prasad 1993, 1994). Consider the propagation of a two-dimensional wavefront in a polytropic gas

https://doi.org/10.1017/S0022112098003310 Published online by Cambridge University Press

which is initially at rest. Such a medium is isotropic and hence the rays are orthogonal to the wavefront. Let $(x(t), y(t))$ be a point which moves along a ray while remaining on the wavefront and $\theta(t)$ be the angle which the ray (i.e. the normal to the wavefront) makes with the x-axis at time t. In two space dimensions the components (n_1, n_1) of the unit normal are $n_1 = \cos\theta, n_1 = \sin\theta$. The high-frequency approximation implies that the leading-order terms in excess density, pressure and the fluid velocity on the wavefront are proportional to an amplitude function w on the wavefront. We first choose w to be of the dimension of velocity. We non-dimensionalize the length and time variables using the velocity a_0 of sound in the medium ahead and a characteristic length L which we choose to be of the order of the distance over which the wave propagates. We also introduce a non-dimensional quantity, Mach number M of the wavefront, by

$$M = \frac{(a_0 + \frac{1}{2}(\gamma+1)w)}{a_0} = 1 + \frac{(\gamma+1)w}{2a_0}. \tag{2.1}$$

In non-dimensional variables the weakly nonlinear ray equations ((4.1)–(4.5) in Prasad, 1994) reduce to

$$\frac{\mathrm{d}x}{\mathrm{d}t} = M\cos\theta, \tag{2.2}$$

$$\frac{\mathrm{d}y}{\mathrm{d}t} = M\sin\theta, \tag{2.3}$$

$$\frac{\mathrm{d}\theta}{\mathrm{d}t} = -\frac{\partial M}{\partial \lambda}, \tag{2.4}$$

where $\partial/\partial\lambda$ is an operator defined by

$$\frac{\partial}{\partial\lambda} = \left(\cos\theta\frac{\partial M}{\partial y} - \sin\theta\frac{\partial M}{\partial x}\right) \tag{2.5}$$

and $\mathrm{d}/\mathrm{d}t$ represents the time rate of change along a nonlinear ray. The transport equation for M coupled to the above equations is

$$\frac{\mathrm{d}M}{\mathrm{d}t} = -\frac{M-1}{2}\frac{\partial\theta}{\partial\lambda}. \tag{2.6}$$

Now, we introduce a ray coordinate system (ξ', t) where $\xi' =$ constant represents the family of rays in the (x, y)-plane and $t =$ constant gives the successive positions of the wavefront. Let g' be the metric such that $g'\mathrm{d}\xi'$ is an element of non-dimensional length along the wavefront at time t. Then due to the orthogonality of the rays and wavefronts, on a given wavefront at time t we have

$$x_{\xi'} = -g'\sin\theta\,, \quad y_{\xi'} = g'\cos\theta\,, \quad g'^2 = \left(x_{\xi'}\right)^2 + \left(y_{\xi'}\right)^2. \tag{2.7a–c}$$

Also from (2.5) and (2.7) we have

$$\frac{\partial}{\partial\xi'} = g'\frac{\partial}{\partial\lambda}. \tag{2.8}$$

In the ray coordinate system (ξ', t), a partial derivative with respect to t represents the time rate of change along a ray i.e. $\partial/\partial t = \mathrm{d}/\mathrm{d}t$. The Jacobian of the transformation from (x, y) to (ξ', t) coordinates has determinant Mg'. Using subscripts to denote partial differentiation, differentiating (2.7c) with respect to t and using (2.2), (2.3) and (2.7a, b) we get

$$g'_t = M\theta_{\xi'}. \tag{2.9}$$

https://doi.org/10.1017/S0022112098003310 Published online by Cambridge University Press

The transport equation (2.6) transforms to

$$\frac{2g'}{M-1}M_t + \theta_{\xi'} = 0. \tag{2.10}$$

Elimination of $\theta_{\xi'}$ from equations (2.9) and (2.10) gives

$$\frac{2g'}{M-1}M_t + \frac{1}{M}g'_t = 0$$

which gives

$$(M-1)^2 \mathrm{e}^{2(M-1)} g' = f(\xi'), \tag{2.11}$$

where f is determined from the distribution of the intensity M on the initial wavefront. When we use equations (2.8) and (2.11) to write the pair of equations (2.4) and (2.6) with ξ' and t as independent variables, the coefficients in these equations depend not only on M but also on ξ'. To get rid of the dependence of the coefficients on ξ' we introduce a new variable $\xi = \int_0^{\xi'} f(\xi')\mathrm{d}\xi'$ so that

$$\frac{\partial}{\partial \xi} = g(M)\frac{\partial}{\partial \lambda}, \tag{2.12}$$

where

$$g(M) = (M-1)^{-2}\mathrm{e}^{-2(M-1)}. \tag{2.13}$$

The equations (2.4) and (2.6) become

$$\theta_t + \frac{1}{g}M_\xi = 0 \tag{2.14a}$$

and

$$M_t + \frac{M-1}{2g}\theta_\xi = 0. \tag{2.14b}$$

Thus the successive positions of the nonlinear wavefront and the distribution of amplitude on it are finally given by (2.2), (2.3) and (2.14). The characteristic curves of equations (2.14) in the (ξ, t)-plane are given by

$$\frac{\mathrm{d}\xi}{\mathrm{d}t} = \pm\left(\frac{M-1}{2g^2}\right)^{1/2}, \tag{2.15}$$

which are real for compression wave, $M-1 > 0$, and purely imaginary for an expansion wave, $M-1 < 0$.

It is well known that different conservation forms of the same equation are not equivalent for a discontinuous solution. The physically realistic conservation form of equations (2.14) is obtained by equating $x_{\xi t}$ with $x_{t\xi}$ and $y_{\xi t}$ with $y_{t\xi}$. This is

$$(g\sin\theta)_t + (M\cos\theta)_\xi = 0, \tag{2.16a}$$

$$(g\cos\theta)_t - (M\sin\theta)_\xi = 0. \tag{2.16b}$$

The above system of equations (2.16) with (2.13), subject to suitable initial conditions (to be described in § 4), form the basic set of equations for our study of propagation of a nonlinear wavefront. The system also provides us with a means of correctly following the movement of kinks on the wavefront.

https://doi.org/10.1017/S0022112098003310 Published online by Cambridge University Press

3. A finite difference scheme

To solve an initial value problem for (2.16) we use a total variation bounded finite difference scheme based on the Lax–Friedrichs flux (Shu 1987; Cockburn, Lin & Shu 1989). The application of this scheme to the above system of conservation laws is based on the decomposition of these equations into characteristic components. The scheme is then applied to individual characteristic components and the solution is obtained from summation of the contributions from the characteristic components.

Consider the conservation law

$$\boldsymbol{u}_t + (\boldsymbol{f}(\boldsymbol{u}))_x = 0, \tag{3.1}$$

where $\boldsymbol{u} = (u_1, \ldots, u_m)^T$, such that the Jacobian matrix $\boldsymbol{A}(\boldsymbol{u}) = \partial \boldsymbol{f}/\partial \boldsymbol{u}$ has m real eigenvalues and a complete set of eigenvectors. On the computational grid $x_j = j\Delta x, \quad t_n = n\Delta t$, we use $\boldsymbol{u}_j^n$ to denote the computed approximation to the exact solution $\boldsymbol{u}(x_j, t_n)$ of (3.1). Let $\boldsymbol{A}_{j+1/2} = (\partial \boldsymbol{f}/\partial \boldsymbol{u})_{\boldsymbol{u}=\boldsymbol{u}_{j+1/2}}$ denote the average Jacobian where $\boldsymbol{u}_{j+1/2} = \frac{1}{2}((\boldsymbol{u}_j + \boldsymbol{u}_{j+1})/2)$. We denote the eigenvalues and left and right eigenvectors of $\boldsymbol{A}_{j+1/2}$ by $\lambda_{j+1/2}^{(p)}$, $\boldsymbol{l}_{j+1/2}^{(p)}$, $\boldsymbol{r}_{j+1/2}^{(p)}$, $p = 1, 2, \ldots, m$, normalized so that

$$\boldsymbol{l}_{j+1/2}^{(p)} \cdot \boldsymbol{r}_{j+1/2}^{(p)} = \delta_{pq}. \tag{3.2}$$

We use the standard notation

$$\Delta_+ \boldsymbol{u}_j = \boldsymbol{u}_{j+1} - \boldsymbol{u}_j, \quad \Delta_- \boldsymbol{u}_j = \boldsymbol{u}_j - \boldsymbol{u}_{j-1}.$$

A semidiscrete method of lines to (3.1) is a system of ODEs

$$\frac{\partial \boldsymbol{u}_j}{\partial t} = -\frac{1}{\Delta x}(\boldsymbol{F}_{j+1/2} - \boldsymbol{F}_{j-1/2}), \tag{3.3}$$

where the numerical flux $\boldsymbol{F}_{j+1/2}$ is defined by

$$\boldsymbol{F}_{j+1/2} = \boldsymbol{F}(\boldsymbol{u}_{j-k+1}, \ldots, \boldsymbol{u}_{j+k}) \tag{3.4}$$

for some positive integer k. $\boldsymbol{F}_{j+1/2}$ is Lipchitz continuous in all its arguments, and satisfies the consistency condition

$$\boldsymbol{F}(\boldsymbol{u}, \ldots, \boldsymbol{u}) = \boldsymbol{f}(\boldsymbol{u}). \tag{3.5}$$

Taking the Euler forward time discretization of (3.3) we get

$$\boldsymbol{u}_j^{n+1} = \boldsymbol{u}_j^n - \lambda(\boldsymbol{F}_{j+1/2}^n - \boldsymbol{F}_{j-1/2}^n), \tag{3.6}$$

where $\lambda = \Delta t/\Delta x$ is called the CFL number. In the TVB modification procedure the numerical flux $\boldsymbol{F}_{j+1/2}$ is replaced by a monotone flux (whose choice is defined later) $\boldsymbol{h}_{j+1/2} = \boldsymbol{h}(\boldsymbol{u}_{j+1/2}^-, \boldsymbol{u}_{j+1/2}^+)$, where $\boldsymbol{u}_{j+1/2}^{\pm} = \boldsymbol{u}(x_{j+1/2}^{\pm}, t)$ are defined suitably subject to some local projection limiting. To compute $\boldsymbol{h}_{j+1/2}$, we first find

$$a^{(p)} = \boldsymbol{l}_{j+1/2}^{(p)} \cdot \boldsymbol{a}, \tag{3.7}$$

where we take $\boldsymbol{a} = \boldsymbol{u}_j^{(0)}, \ \boldsymbol{u}_{j+1}^{(0)}, \ \Delta_- \boldsymbol{u}_j^{(0)}, \ \Delta_+ \boldsymbol{u}_j^{(0)}, \ \Delta_+ \boldsymbol{u}_{j+1}^{(0)}$. We then apply the local projection limit in each characteristic field

$$(\tilde{u}_j)^{(p)} = m((u_j^{(0)})^{(p)}, \ (\Delta_+ u_j^{(0)})^{(p)}, \ (\Delta_- u_j^{(0)})^{(p)}),$$
$$(\tilde{u}_{j+1})^{(p)} = m((u_{j+1}^{(0)})^{(p)}, \ (\Delta_+ u_j^{(0)})^{(p)}, \ (\Delta_+ u_{j+1}^{(0)})^{(p)}),$$

https://doi.org/10.1017/S0022112098003310 Published online by Cambridge University Press

where m is the minmod function, i.e.

$$m(b_1, b_2, \ldots, b_n) = \begin{cases} s.\min_{1\leqslant i\leqslant n} |b_i| , & \text{if } \operatorname{sgn}(b_1) = \operatorname{sgn}(b_2) = \ldots = \operatorname{sgn}(b_n) = s \\ 0 , & \text{otherwise.} \end{cases}$$

We then form

$$(u^-_{j+1/2})^{(p)} = (u^{(0)}_j)^{(p)} + \phi(\tilde{u}_j)^{(p)},$$

$$(u^+_{j+1/2})^{(p)} = (u^{(0)}_{j+1})^{(p)} - \phi(\tilde{u}_{j+1})^{(p)},$$

where ϕ is the limiter, $0 < \phi < 1$. Here $\phi = 0$ gives the Lax–Friedrichs flux. Taking $a = u^{\pm}_{j+1/2}$ we return to the component space using

$$\boldsymbol{a} = \sum_{p=1}^{m} a^{(p)} \boldsymbol{r}^{(p)}_{j+1/2} \tag{3.8}$$

and find $\boldsymbol{f}^{\pm}_{j+1/2} = \boldsymbol{f}(\boldsymbol{u}^{\pm}_{j+1/2})$. Next we compute $(f^{\pm}_{j+1/2})^{(p)}$ from (3.7), and then use any scalar monotone flux in the pth characteristic field, $p = 1, 2 \ldots, m$. Here we have used the local Lax–Friedrichs flux, defined by

$$\begin{aligned} h^{(p)}_{j+1/2} &= h((u^-_{j+1/2})^{(p)}, (u^+_{j+1/2})^{(p)}) \\ &= \tfrac{1}{2}[(f^-_{j+1/2})^{(p)} + (f^+_{j+1/2})^{(p)} - (\alpha_{j+1/2})^{(p)}\{(u^+_{j+1/2})^{(p)} - (u^-_{j+1/2})^{(p)}\}] \end{aligned} \tag{3.9}$$

with

$$\alpha^{(p)}_{j+1/2} = \max(|\lambda^{(p)}_j|, |\lambda^{(p)}_{j+1}|).$$

We finally get $\boldsymbol{h}_{j+1/2}$ by using (3.8), with $a = h_{j+1/2}$:

$$\boldsymbol{h}_{j+1/2} = \sum_{p=1}^{m} h^{(p)}_{j+1/2} \boldsymbol{r}^{(p)}_{j+1/2}.$$

Now, replacing $\boldsymbol{F}_{j+1/2}$ by $\boldsymbol{h}_{j+1/2}$ in (3.6) the total variation bounded finite difference scheme can be written as

$$\boldsymbol{u}^{n+1}_j = \boldsymbol{u}^n_j - \lambda \left[\boldsymbol{h}^n_{j+1/2} - \boldsymbol{h}^n_{j-1/2}\right]. \tag{3.10}$$

The system of conservation laws (2.16) is solved subject to the initial conditions given below.

4. Initial conditions and method of solution

We consider an initially concave wavefront moving from left to right (i.e. in the x-direction) into a gas at rest. Let

$$x(\xi, 0) = x_0(\xi), \quad y(\xi, 0) = y_0(\xi) \tag{4.1}$$

denote the initial wavefront, with an initial distribution of amplitude

$$M(\xi, 0) = M_0(\xi). \tag{4.2}$$

The initial value of θ is obtained from (4.1) as

$$\theta(\xi, 0) = \theta_0(\xi) \tag{4.3}$$

and the initial value of g is obtained from (2.13) as

$$g(\xi, 0) = g(M(\xi, 0)). \tag{4.4}$$

https://doi.org/10.1017/S0022112098003310 Published online by Cambridge University Press

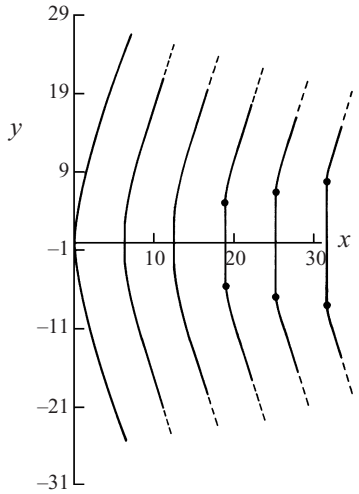


FIGURE 2. Comparison of the solution obtained from the finite difference scheme with the exact composite simple wave solution of the equations of nonlinear ray theory. Here $\theta_0(\xi) = \begin{cases} -0.3 \sin\left(\frac{5}{4}\pi\xi\right), & |\xi| < \frac{2}{5} \\ -0.3\ \frac{\xi}{|\xi|}, & |\xi| > \frac{2}{5}. \end{cases}$ Appropriate Riemann invariants are constant on the upper and lower parts of the initial wavefront and $M_0(\theta_0 = 0) = 1.2628$. ———, Solution from the finite difference scheme. — — —, Exact solution obtained by fitting shocks into a composite simple wave solution. The two solutions cannot be distinguished in the figure.

The system of conservation laws (2.16) subject to initial conditions (4.2)–(4.4) is solved using the finite difference scheme described in the previous section. The governing equations are discretized on a two-dimensional grid along the ξ-direction and t-direction in the (ξ, t)-plane. The effect of step sizes $\Delta\xi$, Δt has been studied to optimize them. The numerical procedure for obtaining the successive wavefronts and the rays is as follows: The solution of (2.16) with (2.13) gives $\theta(\xi, t)$, $M(\xi, t)$ and $g(\xi, t)$ for all $t > 0$. Now along a ray given by $\xi = \xi_0$, by integrating (2.2), (2.3) with initial values given by (4.1) we can find (x, y) at time $t > 0$ on the wavefront at $\xi = \xi_0$. A Simpsons rule was used for the integration. By this procedure we get both the ray (joining points (x, y) on $\xi_0 = \text{const}$, for various values of t) as well as the wavefront (joining end points (x, y) of the rays for various values of ξ_0 at a given t). In order to assess the accuracy of the method we have compared our results with an exact composite simple wave solution described by Prasad (1993).† Figure 2 shows that the wavefronts obtained from this scheme cannot be distinguished in the figure with the exact wavefronts.

Before we start discussing the results from the numerical computation, we would like to point out that the nonlinear ray theory of Choquet-Bruhat and Parker is valid only as long as linear and nonlinear rays are close. Thus their theory, like the linear theory, breaks down before the caustic region (in the linear theory) is reached. Our

† A simple wave solution, an exact solution of the equations (2.14), can be easily computed. We define a composite simple wave to be two simple waves of opposite family separated by a constant state. When the initial wavefront is symmetric about the x-axis, M_0 and θ_0 can be so prescribed that on each half of the wavefront one of the Riemann invariants is constant leading to two simple waves which move apart leaving a constant state in the middle. Shocks (or kinks) can be fitted into both simple waves with the help of the jump relations derived from (2.16). For details see Prasad (1993, pp. 111–113).

https://doi.org/10.1017/S0022112098003310 Published online by Cambridge University Press

WNLRT is based on the geometry of the nonlinear rays and has nothing to do with that of linear rays. Hence our theory is valid over much larger length scale.

5. Results and discussion

In this section we discuss the results of numerical computation of some cases, in which we consider the propagation of a nonlinear wavefront with quite general initial distribution of the amplitude (or intensity). Computations have been carried out by varying the distribution of amplitude along different initial wavefronts. We first consider

5.1. *Case* (*i*): *Propagation of a nonlinear wavefront initially parabolic in shape near the axis of symmetry and straight wings*

Here, the initial wavefront is taken to be a parabola

$$y^2 = bx \quad (2 \leqslant b \leqslant 8), \quad |y| \leqslant z, \quad 0 \leqslant z \leqslant 2 \tag{5.1}$$

and for $|y| > z$ it is extended on the two sides by the corresponding straight lines. Thus for $|y| \geqslant z$, θ_0 is a constant. M_0 is prescribed on the parabola as a symmetric function of θ_0. We take

$$M_0 = \alpha \, \mathrm{e}^{-\beta\theta_0^2} \tag{5.2}$$

where the parameter α is a measure of the strength of the initial wave amplitude and β measures a rate of change of M_0 along the wavefront. Varying α and β we can vary the distribution of amplitude on the wavefront.

5.1.1. *Effects of varying the initial amplitude distribution*

Computations have been carried out for $b = 2, 3, \ldots, 8$. For each value of b, the values of α has been varied between 1.05 and 1.2. We present here the results of only a few representative cases.

Figure 3(*a–d*) shows the propagation of a wavefront with initial position as in (5.1) with $b = 8$ and $z = 2$ and with initial strength given by (5.2) for $\beta = 0.01$ and $\alpha = 1.05, 1.08, 1.1, 1.2$. The nonlinear rays and nonlinear wave-fronts are shown by solid lines and the corresponding linear wavefronts and the linear rays are shown by dotted lines. The geometry of linear wavefronts and linear rays in all the parts of this figure remains unchanged. In figure 3(*a*) for which $M_0 = 1.05$ at the centre, the nonlinear wavefront at $t = 1$ almost coincides with the linear wavefront, but for larger times the nonlinear wavefront moves ahead of the linear wavefront, proving that even small nonlinear effects show up significantly after some time. The linear rays converge and intersect as they approach the central line, so a caustic necessarily forms at a finite time t. The nonlinear rays initially converge, but then, except the central one (being the line of symmetry), deviate significantly from the central line. The nonlinear wavefronts tend to become plane at the centre and the nonlinear rays tend to become parallel to the central ray. Thus, the fronts calculated by our WNLRT do not fold and the rays do not intersect though a pair of kinks with discontinuities in M and θ appear on the wavefront, which are shown as dark points. The initially concave wavefront straightens out to give an ever increasing constant central flat region, bounded by kinks as was also seen in the composite simple wave solution (figure 2).

We also observe that although the linear and nonlinear rays coincide initially, as the linear caustic approaches the nonlinear rays diverge considerably from the linear

https://doi.org/10.1017/S0022112098003310 Published online by Cambridge University Press

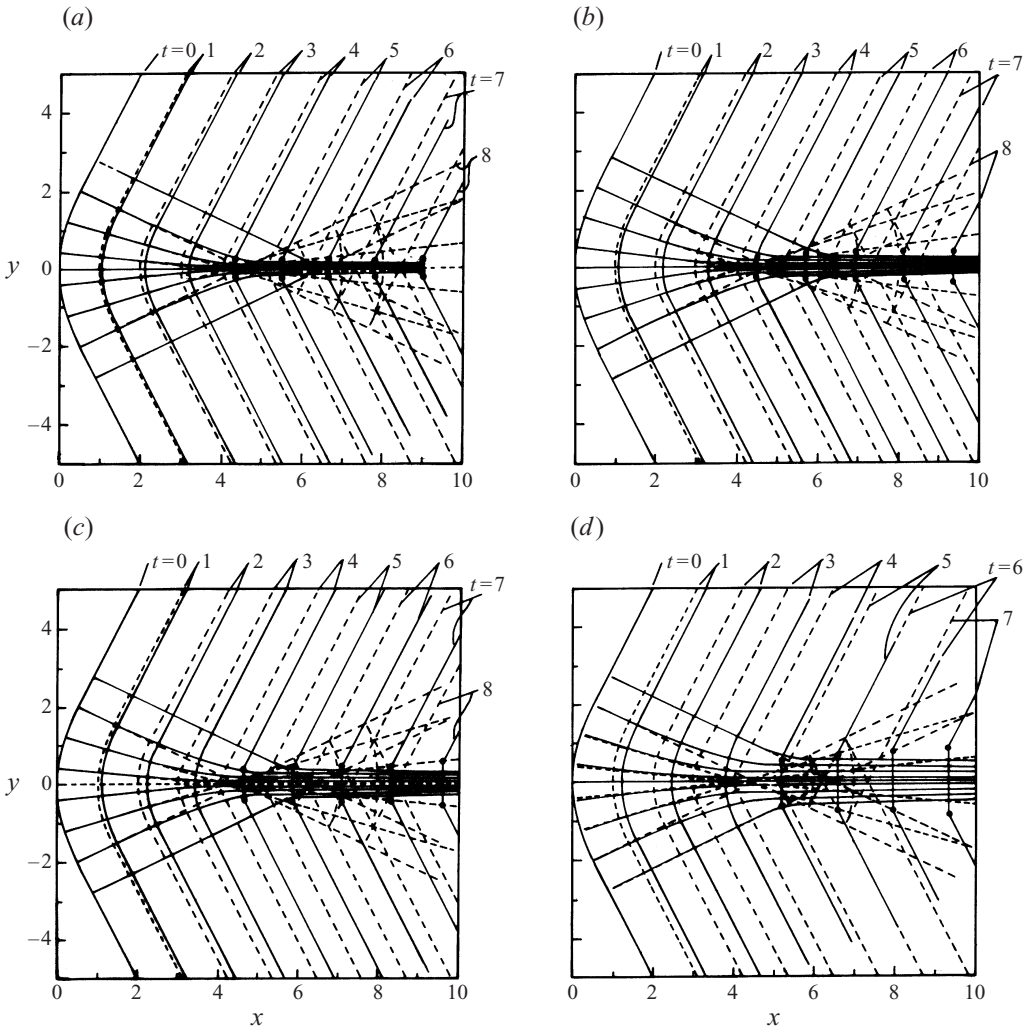


FIGURE 3. Nonlinear wavefronts starting from an initial wavefront in which the central part is the parabola $y^2 = 8x$, for $|y| < 2$. Amplitude distribution is $M_0 = \alpha\, e^{-\beta\theta^2}$. ———, Nonlinear wavefronts and rays. — — —, Linear wavefronts and rays. •, The position of the kink on the nonlinear wavefront. (*a*) $\alpha = 1.05$, (*b*) $\alpha = 1.08$, (*c*) $\alpha = 1.10$, (*d*) $\alpha = 1.20$, $\beta = 0.01$.

rays. As M_0 increases at the centre, this divergence from the linear rays takes place at an earlier time. A closer look at the rays (figure 4) shows that the nonlinear rays successively converge and diverge similar to the rays reported in figure 6(*c*) of Sturtevant & Kulkarny (1976).

The reason for convergence and divergence of rays is seen more clearly by examining the evolution of the amplitude with time corresponding to figure 3(*c*) which is shown in figure 5 (for $\alpha = 1.1$, $\beta = 0.01$). The rays in the central part of the wave-front converge due to a larger curvature there, thus causing the ray tube area to decrease, so that M increases in the central part of the wavefront and attains a maximum at the centre. At $t = 4$ the steep gradient of M causes the central part of the wavefront to move faster than the sides, so that the curvature at the centre decreases resulting in the divergence of the rays. Thus the ray tube area increases and as energy is conserved

https://doi.org/10.1017/S0022112098003310 Published online by Cambridge University Press

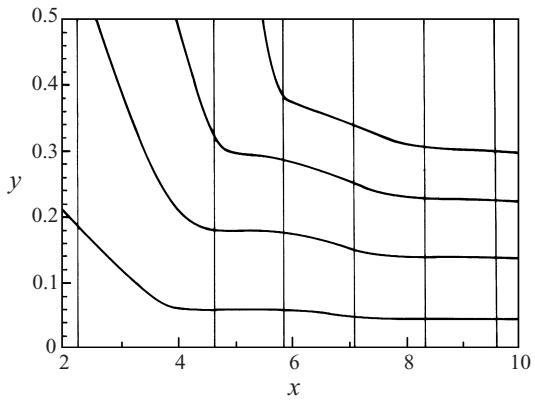


FIGURE 4. A blow up of part of the (x, y)-plane of figure 3(c) showing the convergence and divergence of the nonlinear rays.

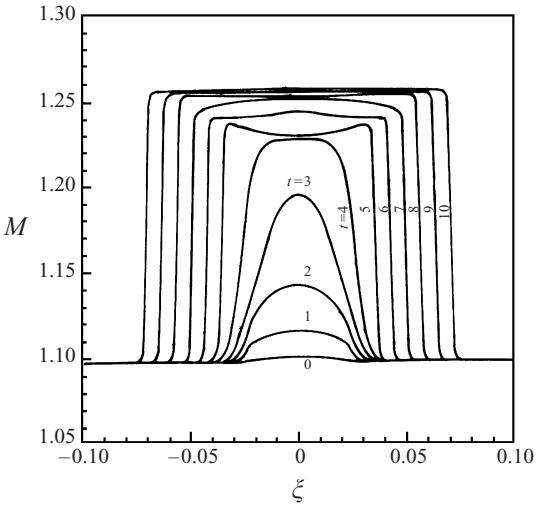


FIGURE 5. Evolution of the Mach number M with time, corresponding to figure 3(c) when $\alpha = 1.1,\ \beta = 0.01$.

along a ray tube the value of M does not increase at the centre as fast as on two sides after $t = 4$. Its shape in the (ξ, M)-plane has a local minimum at $t = 5$ soon after the focus (the point to which the linear rays converge; linear theory predicts infinite amplitude at this point). After this M starts increasing at the centre and the nonlinear rays start converging once again. This process of convergence and divergence repeats successively and will be seen more clearly in figure 10. From $t = 5$, M increases steadily at the centre, and shows a well developed pair of discontinuities in the form of shocks in the (ξ, M)-plane. These discontinuities in M and θ in the (ξ, t)-plane are mapped into a pair of kinks on the wavefront itself. Once the kinks have appeared the intensity of the wavefront in the central flat region does not increase very much and reaches a maximum amplitude M_{max}.

Figure 6(a) shows the plot of $M_{max} - 1$, where M_{max} is the maximum Mach strength attained during the course of numerical solution, against initial Mach strength $M_0 - 1$ at the centre. It shows that $M_{max} - 1$ is a monotonically increasing function of $M_0 - 1$.

https://doi.org/10.1017/S0022112098003310 Published online by Cambridge University Press

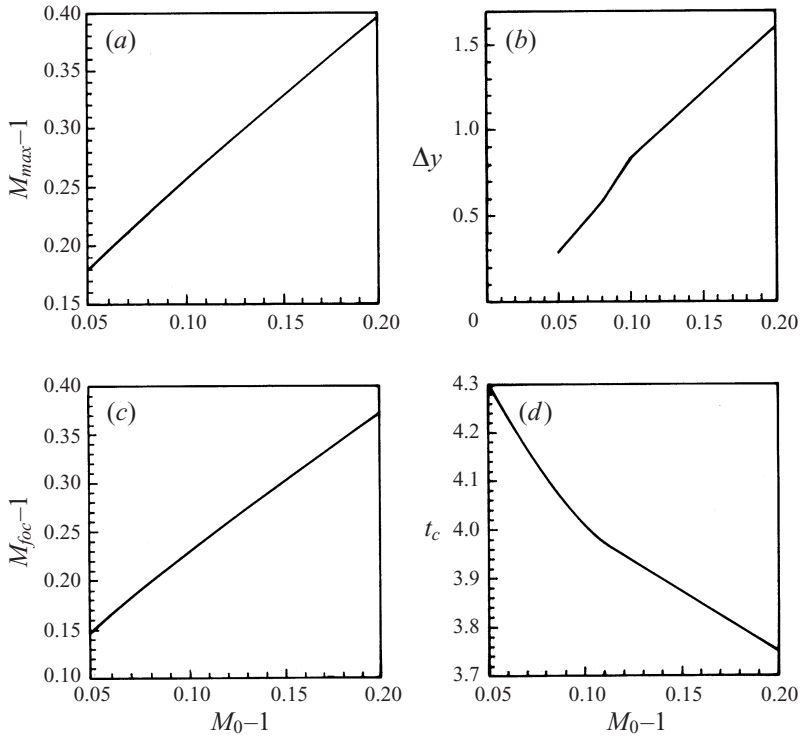


FIGURE 6. (*a*) Maximum amplification of Mach strength as a function of initial Mach strength M_0-1. (*b*) Separation of kinks Δy as a function of initial Mach strength M_0-1. (*c*) M at focus as a function of initial Mach strength M_0-1. (*d*) Critical time of formation of kinks t_c as a function of initial Mach strength M_0-1 on the axis of symmetry. Initial Mach strength M_0 means its maximum value at the centre of symmetry.

The separation of the kinks is also a monotonically increasing function of the initial Mach strength. Figure 6(*b*) shows the plot of the kink separation (Δy), at a particular time, versus the initial Mach strength. Figure 6(*c*) shows the plot of $M-1$ at the focus, i.e. $M_{foc}-1$ against the initial Mach strength M_0-1 on the axis of symmetry. Figure 6(*d*) shows the dependence of the critical time t_c when the kinks first appear on the initial Mach strength. It is observed that as M_0-1 increases, kinks are formed at an earlier time.

In figures 3–6 initial M_0 is so prescribed that it is maximum at the centre of symmetry of the wavefront and decreases to each side. Figure 7(*a*) shows the (x, y) plot at different times when the initial wavefront is the same as in figure 3(*c*), but M_0 is so prescribed that it is minimum at the centre and maximum on the wings. The parameters $\alpha = 1.095$ and $\beta = -0.01115$ are chosen so that the value of M_0 although minimum at the centre coincides in the constant region at the two sides with its value when $\alpha = 1.1$ and $\beta = 0.01$. Figure 7(*b*) depicts the comparison of the evolution of Mach strength with time, in this case with that in figure 5. The solid lines correspond to this case and the dotted lines represent figure 5. The value of M_{max} (when M_0 has a minimum at the centre) is less at $t = 1$ and $t = 2$ but at $t = 10$ both tend to almost the same constant state. Thus, even if M_0 is prescribed to be minimum at the centre it increases immediately due to geometric convergence and its value for larger times does not vary significantly in the two cases. We therefore

https://doi.org/10.1017/S0022112098003310 Published online by Cambridge University Press

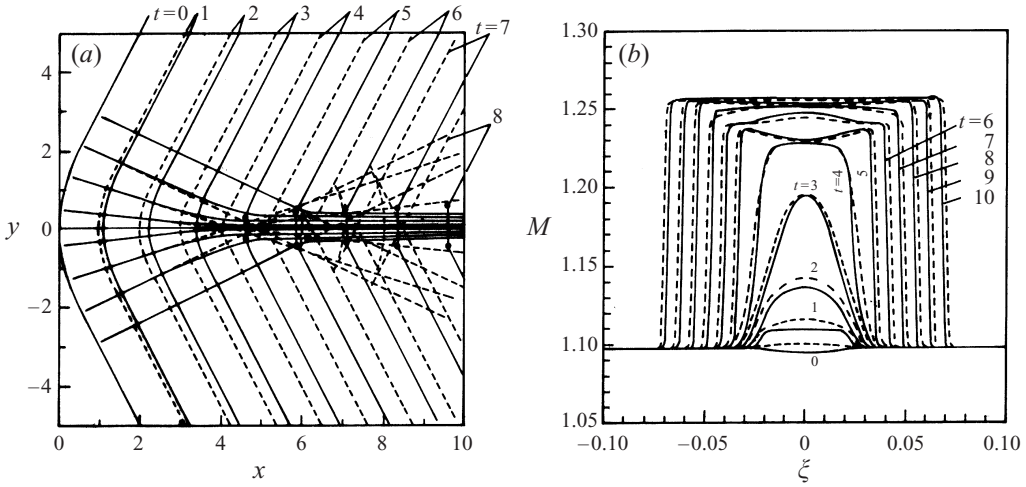


FIGURE 7. (*a*) Nonlinear wavefronts starting from an initial position in which the central part is the parabola $y^2 = 8x$, for $|y| < 2$. Initial amplitude distribution is $M_0 = \alpha e^{-\beta\theta^2}$ where $\alpha = 1.095$, $\beta = -0.01115$. Dotted lines represents the linear wavefront. (*b*) Evolution of Mach number M with time corresponding to (*a*) is compared with figure 5. – – –, M_0 is maximum at the centre, corresponding to the case in figure 3(*c*). ——, M_0 is minimum at the centre, corresponding to the case in (*a*).

conclude that reducing M_0 at the centre without changing its value in the constant region on the two sides produces no noticeable change in the geometry and position of the nonlinear wavefronts and the nonlinear rays, so that figure 7(*a*) and figure 3(*c*) are almost the same. In order to study the effect of varying the gradient of the amplitude along the wavefront we consider the initial wavefront to be the same as in figure 3(*c*), and fixing $\alpha = 1.1$, we vary β from 0 to 0.2. This leads to an increase in the gradient of M especially in the central part and the constant value of M_0 on the wings decreases considerably. The results have been summarized in figure 8(*a–d*). It is observed (not shown in the figure) that as the gradient of the amplitude increases the deviation of the nonlinear rays from the linear rays becomes more pronounced in the central part of the wavefront. As the rays diverge at an earlier time the ray tube area increases which slows down the rate of increase of M. Thus M_{max} and M_{foc} decrease as β increases as shown in figure 8(*a*, *b*). Figure 8(*c*) shows that as β increases the kink separation Δy increases while the critical time of formation of the kinks t_c decreases as seen in figure 8(*d*).

5.1.2. *Effects of varying the initial curvature*

In order to study the effect of varying the curvature of the initial wavefront we have considered the initial wavefront to be as in (5.1) with $b = 4, 6, 8$ and $z = 1$ and show the results in figure 9. In all these cases M_0 is prescribed as in (5.2) with $\alpha = 1.1$ and $\beta = 0$ so that M_0 is constant along the initial wavefront.

We observe that as the curvature increases, i.e. b decreases, the rays tend to converge faster, so that the wave amplitude increases rapidly. Thus M_{max} and M_{foc} increase with decreasing b as shown in figure 9(*a*, *b*). The kink separation Δy also decreases with increasing curvature as shown in figure 9(*c*). Figure 9(*d*) gives the plot of t_c as a function of b showing that as curvature increases kinks are formed earlier.

https://doi.org/10.1017/S0022112098003310 Published online by Cambridge University Press

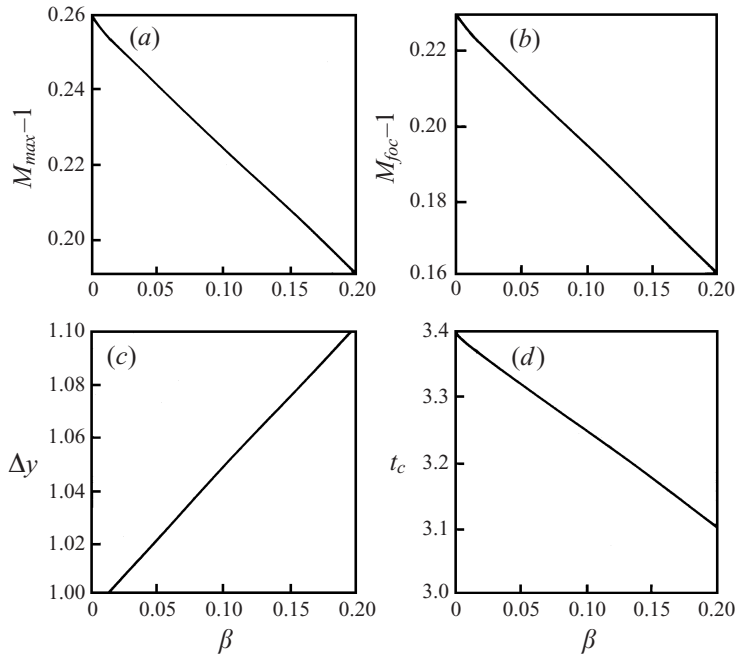


FIGURE 8. Effect of varying the gradient of the amplitude along the initial wavefront. An increase in β corresponds to an increase in the gradient of M along the initial wavefront. (*a*) Maximum amplification of Mach strength, (*b*) M at the focus, (*c*) separation of kinks Δy, (*d*) critical time of formation of kinks t_c.

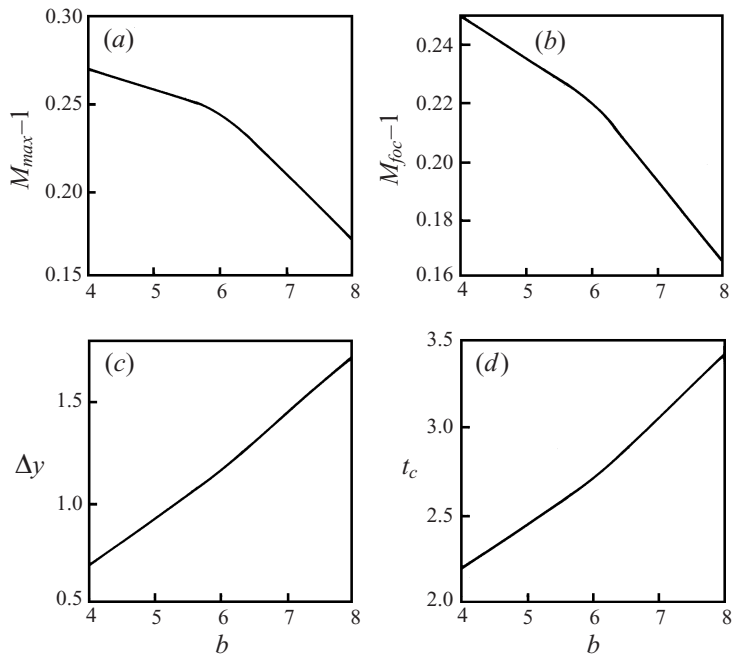


FIGURE 9. Effect of varying the curvature of the initial wavefront. As b decreases the curvature of the initial wavefront increases. (*a*) Maximum amplification of Mach strength, (*b*) M at the focus, (*c*) critical time of formation of kinks t_c, (*d*) separation of kinks Δy.

https://doi.org/10.1017/S0022112098003310 Published online by Cambridge University Press

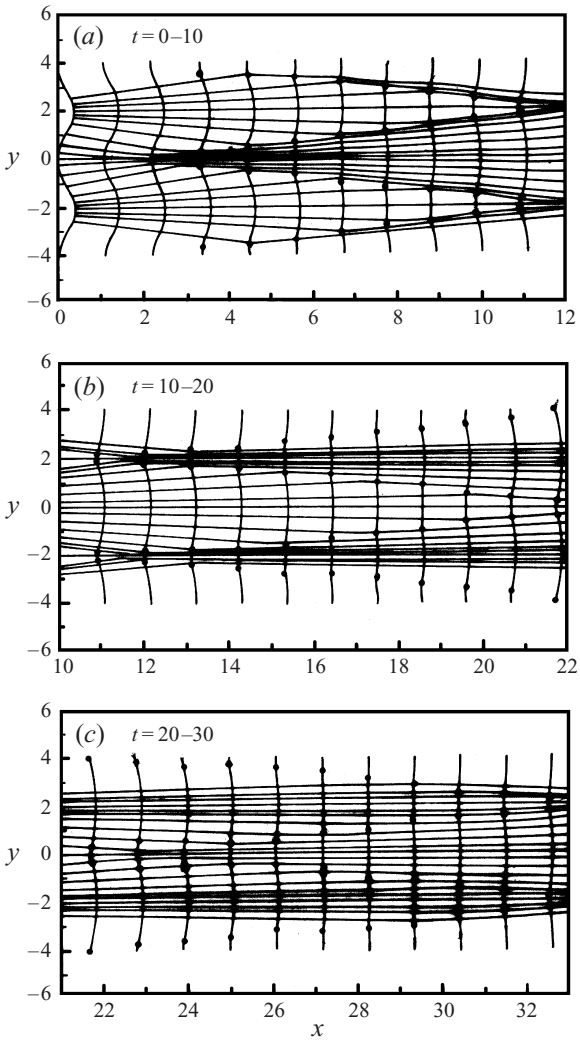


FIGURE 10 (*a–c*). For caption see facing page.

5.2. *Case* (*ii*): *Propagation of a nonlinear wavefront with initially periodic shape*

We first take the initial wavefront to be sinusodial in shape, given by the curve

$$x = 0.2 - 0.2A\cos(\pi y/B)$$

with $A = 1$ and $B = 2$. M_0 is prescribed as in (5.2) with $\alpha = 1.08$, $\beta = 0.08$. Figure 10(*a–e*) shows the nonlinear rays and the nonlinear wavefronts at successive times. With increasing time the nonlinear rays tend to become straight lines parallel to the central line and the nonlinear wavefronts tend to become plane. In this case the convergence and divergence of the rays is seen very clearly. At the beginning the two kinks (shown by dark points on the wavefronts) nearest to the x-axis move away from one another, then they start approaching the kinks on either side, and interact producing a new pair of kinks and this process continues. The amplitude becomes almost a constant and the wavefront becomes plane. The variation of amplitude with time is shown in figure 11. Let $M_{max}(t)$ and $M_{min}(t)$ represent the maximum and

https://doi.org/10.1017/S0022112098003310 Published online by Cambridge University Press

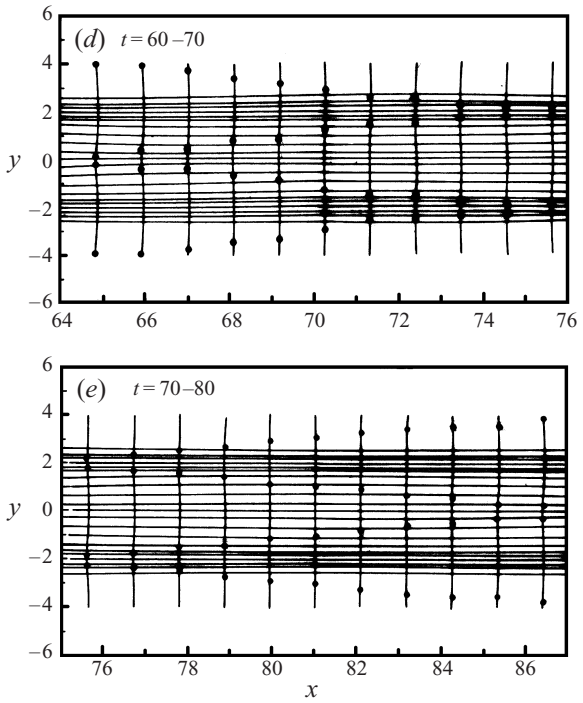


FIGURE 10. Geometry and position at successive times of a nonlinear wavefront with initially sinusoidal shape $x = 0.2 - 0.2A\cos(\pi y/B)$, $A = 1$ and $B = 2$. $M_0 = \alpha e^{-\beta\theta^2}$ with $\alpha = 1.08$ and $\beta = 0.08$. The rays successively converge and diverge. •, The position of the kink on the nonlinear wavefront.

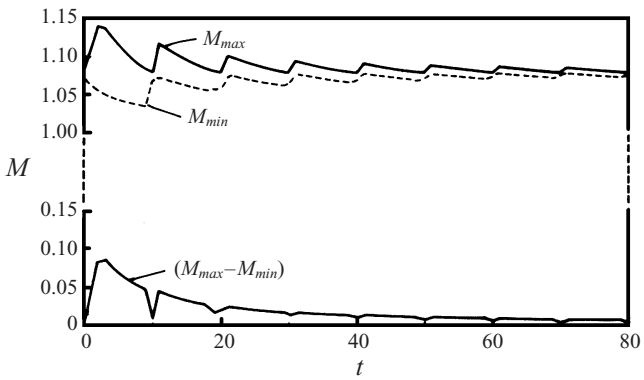


FIGURE 11. Variation of $M_{max}(t)$ and $M_{min}(t)$ with time when the initial wavefront is of sinusoidal shape. $M_{max}(t) - M_{min}(t) \to 0$ as $t \to \infty$

minimum Mach strength obtained at a given time t, then figure 11 shows the graphs of $M_{max}(t)$, $M_{min}(t)$ and $M_{max}(t) - M_{min}(t)$ with t for $M_{max}(0) = 1.08$. The functions $M_{max}(t)$ and $M_{min}(t)$ oscillate but approach a constant value asymptotically. The difference $M_{max}(t) - M_{min}(t) \to 0$ as $t \to \infty$.

We next consider the initial wavefront to be periodic but of an arbitrary shape with positive and negative curvature in each period. Figure 12 shows the nonlinear rays and nonlinear wavefronts corresponding to this case at successive times. As for

https://doi.org/10.1017/S0022112098003310 Published online by Cambridge University Press

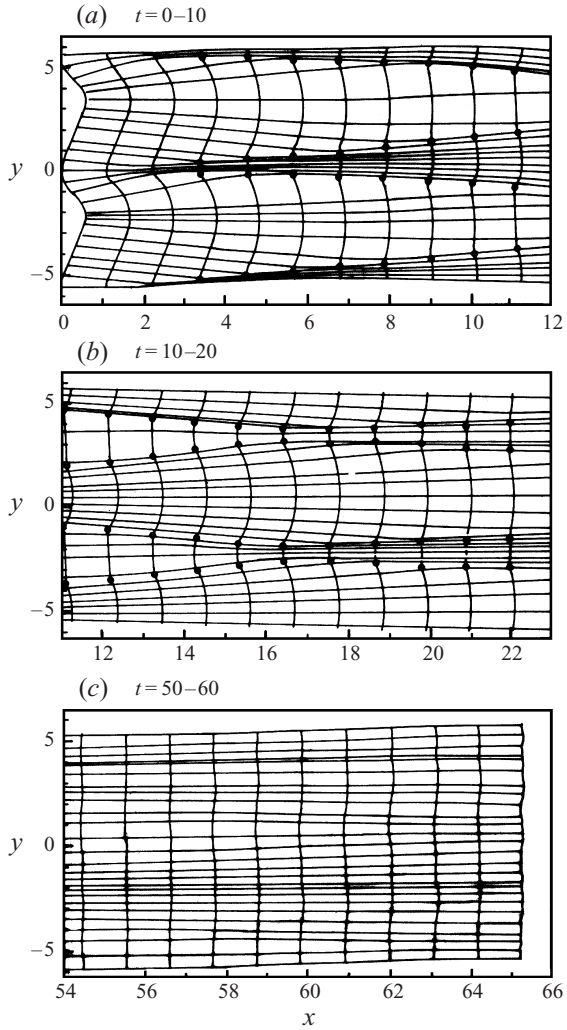


FIGURE 12. Geometry and position at different times of a nonlinear wavefront, where the initial wavefront is a periodic curve with an alternating sequence of positive and negative curvature. $M_0 = 1.06$ along the initial wavefront. The nonlinear wavefronts tend to become plane and the nonlinear rays tend to become straight lines parallel to the x-axis. •, The position of the kink on the nonlinear wavefront.

a sinusoidal front in this case too the two kinks nearest to the x-axis first move away from one another, then they start approaching the kinks on either side and interact producing a new pair of kinks. Results show that even this front has the same flattening and self-stabilizing property as the sinusoidal wavefront so that for larger times the nonlinear rays tend to become straight lines parallel to the x-axis and the amplitude distribution tends to become uniform.

The properties observed above are generic properties of a weakly nonlinear wavefront and there is every reason to believe these properties to be true also in the case of a shock front leading to its corrugational stability. First, we notice that an isolated shock and hence a kink, once formed, persist for all time (see Prasad, 1993, § 1.5). Further, we notice from the two examples that two kinks on an initially periodic

https://doi.org/10.1017/S0022112098003310 Published online by Cambridge University Press

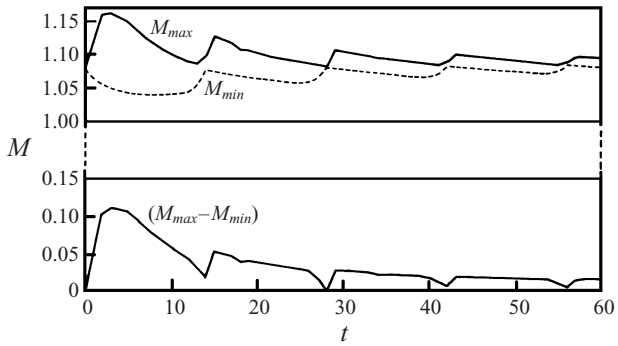


FIGURE 13. Variation of $M_{max}(t)$ and $M_{min}(t)$ with time when the initial wavefront is a periodic curve with an alternating sequence of positive and negative curvature. $M_{max}(t) - M_{min}(t) \to 0$ as $t \to \infty$.

wavefront interact and produce another pair of kinks. Therefore, there is every reason to believe that kinks persist for all time even if $M_{max}(t) - M_{min}(t) \to 0$ (figure 13). The property that a periodic wavefront tends to become plane is due to dissipation of the kinetic energy associated with the wavefront – the source of this dissipation being the kinks, which persist for all time. Some work on this is in progress which we shall report later. A mathematical proof of the smoothing or corrugational stability of a nonlinear wavefront comes from the classical work of Glimm & Lax (1970) on the asymptotic form of the periodic solutions of a pair of conservation laws of which (2.16) is a particular case. According to this result if the initial data are periodic, the oscillations in the solution decays like $1/t$ and the solution itself approaches a function which is the mean value of the solution per period. Thus, $M_{max}(t) - M_{min}(t) \to 0$ as $t \to \infty$.

6. Conclusion

The numerical results presented in this paper demonstrate that the nonlinear effects in gas dynamics not only limit the maximum amplitude of a wavefront in the caustic region of the linear thoery but also bring about a considerable change in the wavefront geometry at and beyond the focus. The geometry, position and amplitude of a nonlinear wavefront depends on the initial position of the wavefront, its amplitude and the gradient of the amplitude on it. Numerical experiments with different initial shapes and different values of the initial amplitude distribution reveal that in no case does the amplitude increase so much that the small-amplitude assumption is violated. This is in contrast to the linear theory, where at the focus infinite amplitude is predicted by its leading-order terms and very large amplitude is predicted when the next order terms are included (Buchal & Keller 1962).

The authors sincerely thank Professor K. W. Morton and Dr Veerappa Gowda for valuable discussions.

REFERENCES

BUCHAL, R. N. & KELLER, J. B. 1960 Boundary layer problems in diffraction theory. *Comm. Pure Appl. Maths* **13**, 85–114.

CHOQUET-BRUHAT, Y. 1969 Ondes asymptotiques et approachées pour des systémes d'equations aux dérivées partielles nonlinéaires. *J. Maths Pures Appl.* **48**, 117–158.

https://doi.org/10.1017/S0022112098003310 Published online by Cambridge University Press

Cockburn, B., San-Yih, Lin & Shu, C. W. 1989 TVB Runge-Kutta local projection discontinuous Galerkin finite element method for conservation laws III: One- dimensional systems. *J. Comput. Phys.* **84**, 90–113.

Friedlander, F. G. 1958 *Sound Pulses*. Cambridge University Press.

Glimm, J. & Lax, P. D. 1970 *Decay of Solutions of System of Nonlinear Hyperbolic Conservation Laws*. American Mathematical Society, Providence, Rhode Island.

Kay, I. and Keller, J. B. 1954 Asymptotic evaluation of a field at a caustic. *J. Appl. Phys.* **25**, 876–883.

Kevlahan, N. K.-R. 1994 Structure and shocks in turbulence. PhD Thesis, University of Cambridge.

Kevlahan, N. K.-R. 1996 The propagation of weak shocks in non-uniform flows. *J. Fluid Mech.* **327**, 161–197.

Morton, K. W., Prasad, P. & Ravindran, R. 1992 Conservation forms of nonlinear ray equations. *Tech. Rep.* 2, Dept. Mathematics Indian Institute of Science.

Parker, D. F. 1969 Nonlinearity, relaxation and diffusion in acoustics and ultrasonics. *J. Fluid Mech.* **39**, 793–815.

Parker, D. F. 1971 An asymptotic theory for oscillatory nonlinear signals. *J. Inst. Maths Applics.* **7**, 92–110.

Prasad, P. 1975 Approximation of perturbation equations of a quasilinear hyperbolic system in the neighbourhood of a bicharacteristic. *J. Math. Anal. Applics.* **50**, 470–482.

Prasad, P. 1993 *Propagation of a Curved Shock and Nonlinear Ray Theory*. Longman, Pitman Research Notes in Mathematics 293.

Prasad, P. 1994 A nonlinear ray theory. *Wave Motion* **20**, 21–31.

Prasad, P. 1995 Formation and propagation of singularities on a nonlinear wavefront and a shock front. *J. Indian Institute of Science, Special volume on Fluid Mechanics* **75**, 537–558.

Ramanathan, T. M. 1985 Huygens' method for constuction of weakly nonlinear wavefronts and shockfronts with application to hyperbolic caustic. PhD Thesis, Indian Institue of Science, Bangalore.

Ravindran, R. & Prasad, P. 1985 Kinematics of a shock front and resolution of a hyperbolic caustic. *Advances in Nonlinear Waves*, Vol. II (ed. L. Debnath) Pitman Research Notes in Mathematics, pp. 77–79.

Rosales, R. R. 1991 An introduction to weakly nonlinear geometrical optics. In *Multi-dimensional Hyperbolic Problems and Computations*, Vol. 29, IMA volumes in Mathematics and its Applications, editors J. Glimm and A. J. Majda, Springer-Verlag, New York 281–310.

Shu, C. W. 1987 TVB uniformly higher order schemes for conservation laws. *Math. Comput.* **49**, 105–121.

Strutevant, B. & Kulkarny, V. A. 1976 The focusing of weak shock waves. *J. Fluid Mech.* **73**, 651–671.

Whitham, G. B. 1957 A new approach to problems of shock dynamics. Part 1, Two-dimensional problems. *J. Fluid Mech.* **2**, 146–171.

Whitham, G. B. 1974 *Linear and Nonlinear Waves*. John Wiley and Sons.

https://doi.org/10.1017/S0022112098003310 Published online by Cambridge University Press